Acknowledgment. The research reported above represents part of the senior author's Ph.D. dissertation at the University of California, Berkeley. This research was supported by the National Science Foundation (NSF Grants EAR 81-15859 and EAR 8606052), the Department of Energy (DOE Contract DE-AT03-83ER-13100 and DOE Grant DE-FG03-85ER-13419), and The Committee on Research at the University of California, Berkeley. We are indebted to Peter C. Lichtner, Everett L. Shock, Barbara L. Ransom, William M. Murphy, Leo Brewer, George H. Bremhall, William L. Marshall, and Dimitri Sverjensky for helpful discussions, encouragement, and assistance during the course of this study. Thanks are also due Kim Suck-Kyu for drafting figures, Joachim Hampel for photographic assistance, and Tony Wong for his computer expertise.

Appendix A

Shedlovsky[23] proposed the equation

$$\alpha_n = \frac{\Lambda_\epsilon}{\Lambda^\circ_e} + \left(\frac{A_\Lambda \Lambda^\circ_e + B_\Lambda}{\Lambda^{\circ 2}_e}\right) \Lambda_\epsilon (I\alpha_n)^{1/2} \qquad \text{(A-1)}$$

to calculate the degree of dissociation of electrolyte solutions. Dividing both sides of eq A-1 by Λ_ϵ and combining with eq 8 yields

$$\frac{1}{\Lambda_e} = \frac{1}{\Lambda^\circ_e} + \left(\frac{A_\Lambda \Lambda_e + B_\Lambda}{\Lambda^{\circ 2}_e}\right) (I\alpha_n)^{1/2} \qquad \text{(A-2)}$$

Substituting eq 6 into eq A-2 and multiplying both sides by Λ°_e results in

$$\frac{\Lambda^\circ_e}{\Lambda_e} = 1 + \frac{1}{\Lambda^\circ_e}(A_\Lambda \Lambda^\circ_e + B_\Lambda) I^{1/2} \qquad \text{(A-3)}$$

which can be rearranged to give eq 9.

Registry No. NaCl, 7647-14-5; NaBr, 7647-15-6; NaI, 7681-82-5; KCl, 7447-40-7; KBr, 7758-02-3; KI, 7681-11-0; CsCl, 7647-17-8; CsBr, 7787-69-1; CsI, 7789-17-5; RbF, 13446-74-7; RbCl, 7791-11-9; RbBr, 7789-39-1; RbI, 7790-29-6; LiCl, 7447-41-8.

(32) Sverjensky, D. A.; Shock E. L.; Helgeson H. C., submitted for publication in *Geochim. Cosmochim. Acta.*

Laboratory-Frame Cross-Correlation Functions in Molecular Liquids Induced by External Fields

M. W. Evans†

Department of Chemistry, University College of Wales, Aberystwyth SY23 1NE, Wales
(Received: July 1, 1987; In Final Form: September 17, 1987)

It is shown by computer simulation that new types of statistical cross correlation appear in the laboratory frame in molecular liquids subjected to external fields of force. New types of time cross-correlation functions are established (i) with an external homogeneous field; (ii) via linear flow induced by an externally applied inhomogeneous electric field; (iii) via vortex flow set up by a rotating external electric field. A simple analytical theory is developed to establish the probable effect of strong cross correlations between linear and angular momentums on the absorption and dispersion spectra of the molecular angular velocity at microwave and far-infrared frequencies.

Introduction

The recent discovery has been made that new types of fundamental time cross-correlation functions (ccf's) become observable in molecular liquids when the overall isotropy of the sample is removed by an external field of force.[1] The ccf

$$C_1(t) = \langle \mathbf{v}(t)\omega^T(0)\rangle$$

was characterized for the first time by computer simulation. Here $\mathbf{v}(t)$ is the molecular center of mass linear velocity and ω the angular velocity of the same molecule. Both vectors are defined in the laboratory frame of reference. An analytical theory has been developed[1] for $C_1(t)$ based on the Langevin equation for rototranslational molecular diffusion in the presence of a homogeneous external electric field. Both the computer simulation and the theory showed clearly that the liquid sample was also birefringent; e.g., the angular velocity and rotational velocity autocorrelation functions (acf's) in the presence of a z-axis field had a different time dependence in the z and x axes of laboratory frame. This leads to the conclusion that the techniques available[2,3] for the study of electric (or magnetic) field induced birefringence in molecular liquids or liquid crystals can also be used to observe fundamental new ccf's such as C_1. A mathematical relation was provided between the observable elements of the matrix C_1 and the angular velocity acf's in the z and x axes of the laboratory frame.

In this paper this work is extended in two directions. First, it is shown that far-infrared power absorption spectra[4-6] from the computer simulation have a different frequency dependence in the z and x axes of the laboratory frame in the presence of a z axis homogeneous electric field. This property is related, through the fundamental equations of motion, to the appearance of C_1 in the laboratory frame and also to new types of direct statistical correlation between the time derivative of the dipole moment μ and its own linear velocity $\mathbf{v}$. Elements of the new ccf matrix

$$C_2(t) = \langle \mu(t)\mathbf{v}^T(0)\rangle$$

also exist therefore in the laboratory frame in the presence of birefringence. It follows that a careful measurement of the far-infrared power absorption spectrum parallel and perpendicular to the external electric field provides information on these fundamental ccf's.

† Present address: Department 48B/428, IBM Data Systems Division, Neighborhood Rd., Kingston, NY 12401, and Visiting Academic, Department of Microelectronics and Electrical Engineering, Trinity College, Dublin 2, Republic of Ireland.

(1) Evans, M. W. *Phys. Rev. A* **1984**, *30*, 2062; *Physica B* **1985**, *131B*, 273.
(2) Kielich, S. In *Dielectric and Related Molecular Processes*; ed. Davies, M., Ed.; Chemical Society: London, 1972; Vol. 1.
(3) Beevers, M. S.; Elliott, D. A. *Mol. Cryst. Liq. Cryst.* **1979**, *26*, 411.
(4) Evans, M. W.; Evans, G. J.; Coffey, W. T.; Grigolini, P. *Molecular Dynamics*; Wiley/Interscience: New York, 1982.
(5) Coffey, W. T.; Evans, M. W.; Grigolini, P. *Molecular Diffusion*; Wiley/Interscience: New York, 1984.
(6) *Memory Function Approaches to Stochastic Problems in Condensed Matter*; Evans, M. W.; Grigolini, P.; Pastori-Parravicini, G., Eds.; Prigogine, I.; Rice, S. A., Series Eds.; Wiley/Interscience: New York, 1985.

0022-3654/88/2092-1639$01.50/0

Second, we extend the computer simulation analysis to flow birefringence. The well-developed methods of fluid mechanics[7] may be used to show that inhomogeneous and rotating electric fields involve linear and vortex flow respectively in a molecular (structured) liquid. An electric field gradient $\nabla\mathbf{E}$ produces a direct body force[9] on a dipolar molecule of moment μ. The effective microscopic field $\mathbf{E}$ itself produces a direct torque

$$-\mu \times \mathbf{E}$$

but we show that there is also an additional indirect torque due to the effective field gradient $\nabla\mathbf{E}$. This is discussed further in this paper where it is demonstrated that the fluid flow due to the effective field gradient produces birefringence which results in the appearance of new ccf's such as C_1. It follows that these fundamental ccf's appear in a molecular liquid whenever there is flow. This appearance of laboratory-frame ccf's is therefore a natural consequence of flow birefringence.

If a molecular liquid is enclosed in a thin-walled glass sphere suspended on a torsion wire between four metal plates and if a rotating electric field is applied with these plates, there appears an experimentally measurable torque in the torsion wire, whose magnitude depends on the field frequency and on the nature of the molecular liquid itself. Born[8] demonstrated in 1920 that this torque is maximized at the point

$$\omega\tau = 1$$

where ω is the angular frequency (rad s^{-1}) of the rotating electric field and τ is the Debye relaxation time. Using a new hydrodynamic approach appropriate to "structured" media (i.e., molecular liquids), Dahler[9] has extended the work of Born to explain the early data of Lertes.[10] The macroscopic torque measured by Lertes is produced by a vortex flow set up in the molecular liquid by the rotating electric field. This vortex produces the torque on the walls of the glass sphere, the walls producing a boundary condition for the hydrodynamic equations of the structured fluid (the molecular liquid). In this paper we attempt an explanation of this phenomenon with a fundamental molecular approach, based on computer simulation. The little-known work of Lertes[10] and the later measurements of Grossetti[11] are important in the context of molecular liquid and liquid crystal dynamics, because these measurements clearly show that a weak external electric field can produce easily measurable macroscopic effects in a molecular liquid. These effects are not confined exclusively to nematogens, therefore.[4] In this paper we look for effects in the computer simulation due to rotating and inhomogeneous electric fields applied to liquid dichloromethane at 296 K in a computer simulation.

Torque and Force Due to an Electric Field Gradient

Dahler[9] has discussed the nature of this center of mass linear force density ($\mathbf{F}_0$) and torque density ($\mathbf{Tq}_0$) on a molecule in a structured fluid environment. These are

$$\mathbf{F}_0 = \mathbf{P}_0 \cdot (\nabla\mathbf{E}_0)^{\mathrm{T}} \tag{1}$$

where

$$\mathbf{P}_0 = \langle \sum_{i=1}^{N} q\mathbf{r}_i \, \delta(R_i - R) \rangle \tag{2}$$

and

$$\mathbf{Tq}_0 = -\mathbf{P}_0 \times \mathbf{E}_0 \tag{3}$$

where $\mathbf{E}_0$ is the applied external electric field.

Here $\mathbf{P}_0$ is the polarization density, $q|\mathbf{r}_i|$ the magnitude of the molecular dipole moment on the ith molecule, R_i the location of the center of mass of the ith molecule, R a fixed point in 3-D space, and $\delta(x)$ the Diraq delta function. $(\nabla\mathbf{E}_0)^{\mathrm{T}}$ is the transpose of the dyadic $\nabla\mathbf{E}_0$.

The single molecule counterparts of the hydrodynamic body force and torque

$$\mathbf{F} = \mu \cdot (\nabla\mathbf{E})^{\mathrm{T}} \tag{4a}$$

and

$$\mathbf{Tq} = -\mu \times \mathbf{E} \tag{4b}$$

must be used in the computer simulation to generate ccf's.[5] If the externally imposed electric field gradient is large in comparison with the field itself, then the force $\mathbf{F}$ dominates the interaction energy between the external electric field (imposed with charged condenser plates of the right design) and molecular liquid. In this limit the liquid will flow rapidly as observed recently by G. J. Evans.[12,13] The dyadic may be written as

$$\nabla\mathbf{E} = \left(\frac{\mathrm{d}}{\mathrm{d}x}\mathbf{i} + \frac{\mathrm{d}}{\mathrm{d}y}\mathbf{j} + \frac{\mathrm{d}}{\mathrm{d}z}\mathbf{k}\right)(E_x\mathbf{i} + E_y\mathbf{j} + E_z\mathbf{k}) = \frac{\mathrm{d}E_x}{\mathrm{d}x}\mathbf{ii} + \frac{\mathrm{d}E_y}{\mathrm{d}x}\mathbf{ij} + \frac{\mathrm{d}E_z}{\mathrm{d}x}\mathbf{ik} + \frac{\mathrm{d}E_x}{\mathrm{d}y}\mathbf{ji} + \frac{\mathrm{d}E_y}{\mathrm{d}y}\mathbf{jj} + \frac{\mathrm{d}E_z}{\mathrm{d}y}\mathbf{jk} + \frac{\mathrm{d}E_x}{\mathrm{d}z}\mathbf{ki} + \frac{\mathrm{d}E_y}{\mathrm{d}z}\mathbf{kj} + \frac{\mathrm{d}E_z}{\mathrm{d}z}\mathbf{kk}$$

so that

$$\mathbf{F} = \left(\frac{\mathrm{d}E_x}{\mathrm{d}x}\mu_x + \frac{\mathrm{d}E_x}{\mathrm{d}y}\mu_y + \frac{\mathrm{d}E_x}{\mathrm{d}z}\mu_z\right)\mathbf{i} + \left(\frac{\mathrm{d}E_y}{\mathrm{d}x}\mu_x + \frac{\mathrm{d}E_y}{\mathrm{d}y}\mu_y + \frac{\mathrm{d}E_y}{\mathrm{d}z}\mu_z\right)\mathbf{j} + \left(\frac{\mathrm{d}E_z}{\mathrm{d}x}\mu_x + \frac{\mathrm{d}E_z}{\mathrm{d}y}\mu_y + \frac{\mathrm{d}E_z}{\mathrm{d}z}\mu_z\right)\mathbf{k} \tag{5}$$

where $\mathbf{i}$, $\mathbf{j}$, and $\mathbf{k}$ are unit vectors in the x, y, and z directions of the laboratory frame.

If we assume for simplicity that the externally applied field has only one effective gradient

$$\frac{\mathrm{d}E_z}{\mathrm{d}z}$$

then the translational force on the molecule is purely in the z direction of the laboratory frame, i.e.

$$\mathbf{F} = \frac{\mathrm{d}E_z}{\mathrm{d}z}\mu_z\mathbf{k} \tag{6}$$

Note, however, that there is no difficulty in principle in including in a computer simulation all three gradients of an applied uniaxial electric field.

The force defined in eq 6 is a linear force on the molecular center of mass and therefore produces an equal acceleration on each atom of the molecule. This results indirectly in a net torque as follows. Consider a molecule made up of three atoms, A, B, and C, positioned in the laboratory frame with coordinates (x_A, y_A, z_A), (x_B, y_B, z_B), and (x_C, y_C, z_C). Let the net, indigeneous, intermolecular force on each atom be (F_{xA}, F_{yA}, F_{zA}), (F_{xB}, F_{yB}, F_{zB}), and (F_{xC}, F_{yC}, F_{zC}). The x, y, and z components of the intermolecular torque are then

$$T_x = y_AF_{zA} - z_AF_{yA} + y_BF_{zB} - z_BF_{yB} + y_CF_{zC} - z_CF_{yC} \tag{7}$$

$$T_y = z_AF_{xA} - x_AF_{zA} + z_BF_{xB} - x_BF_{zB} + z_CF_{xC} - x_CF_{zC} \tag{8}$$

$$T_z = x_AF_{yA} - y_AF_{xA} + x_BF_{yB} - y_BF_{xB} + x_CF_{yC} - y_CF_{xC} \tag{9}$$

In these equations there are no force components in the z direction of the laboratory frame so that the effect of the orientation-dependent gradient force, eq 6, modifies the T_x and T_y components of eq 7–9 but not the T_z component. This implies

(7) Dahler, J. S.; Scriven, L. E. *Proc. R. Soc. London, A* **1963**, *275*, 504.
(8) Born, M. *Z. Phys.* **1920**, *1*, 221.
(9) Dahler, J. S. In *Research Frontiers in Fluid Dynamics*; Seeger, R. J.; Temple, G., Eds.; Interscience: New York, 1965.
(10) Lertes, P. *Z. Phys.* **1921**, *4*, 315; *Z. Phys.* **1921**, *6*, 56; *Z. Phys.* **1921**, *22*, 621.
(11) Grossetti, *Nuovo Cimento* **1958**, *10*, 193; *Nuovo Cimento* **1959**, *13*, 621.
(12) Evans, G. J. *J. Chem. Soc., Faraday Trans. 2*, **1983**, *79*, 547, 833. Evans, G. J.; Evans, M. W. *J. Mol. Liq.* **1984**, *29*, 11.
(13) Costa-Ribeiro, J. *Acad. Bras. Sci. An.* **1950**, *22*, 325.

that the net molecular torque is supplemented by extra accelerations of the type

$$\frac{F_{zA}^{(1)}}{m_A} = \frac{1}{M}\frac{dE_z}{dz}\mu_z|k| = \frac{F_{zB}^{(1)}}{m_B} = \frac{F_{zC}^{(1)}}{m_C} \quad (10)$$

where

$$M = m_A + m_B + m_C$$

is the molecular mass.

On average because of the initial isotropy of the molecular liquid sample

$$\langle \delta T_x \rangle = \langle \delta T_y \rangle$$

and this implies that the natural intermolecular torque components T_x, T_y, and T_z are supplemented by an extra torque which acts on each molecule in exactly the same way as a torque of the form[15]

$$|\mathbf{E}| = E_z$$

$$\mu \times \mathbf{E} = \mathbf{i}\mu_y E_z + \mathbf{j}\mu_x E_z$$

Therefore, it follows that an electric field gradient can induce birefringence as a consequence of the unidirectional flow set up by the force, eq 6. Note that there is no torque generated by a force such as eq 6 in the absence of intermolecular forces, i.e., in the special case

$$T_x = T_y = T_z = 0$$

of an infinitely dilute gas. This explains in outline the recent observations made by G. J. Evans,[12,14] who induced flow in molecular liquids using electric fields with steep gradients, i.e., inhomogeneous fields. This led to the discovery of the inverse of the Costa Ribeiro thermodielectric effect and to a new crystal growing technique.[12-14]

Equation 6 was used in this paper to simulate by computer the induction of birefringence in a three-site atom–atom model of dichloromethane,[15] where the effective torque generated from eq 6 is that of eq 10, with A = CH_2 and B = C = Cl.

Rotating Electric Field

The purpose of simulating on the computer the vortex flow set up by a rotating electric field is to make the first attempt in this context to bridge the gap that still exists between the hydrodynamical and molecular-dynamical descriptions. The equation of a rotating electric field is similar to that of a circularly polarized electromagnetic field with the magnetic component removed. Zeldovich et al.[16] have recently reported that a field of this type may be used to separate physically two enantiomers from a racemic mixture through the intermediacy of a cross-correlation function $C_1(t)$ generated by a circularly polarized radio-frequency field. This has direct technological application, and it has also been shown recently that the Pasteur racemic modification can be explained in terms of moving frame cross correlations[1] between rotation and translation.

Dahler discussed the hydrodynamic vortex flow set up by a rotating electric field of the form[9]

$$\mathbf{E} = \mathbf{E}_0 \,\mathrm{Re}\,((\mathbf{i} + i\mathbf{j})e^{-i\omega t}\sin\psi + \mathbf{k}\cos\psi) \quad (11)$$

This type of external electric field precesses about the z axis of the laboratory frame at a constant inclination ψ and an angular velocity ω. In the computer simulation it is possible to increase the frequency to the far-infrared range, and therefore extend to high frequency the experimental measurements of Lertes[10] reported in 1921. In order to simplify the analysis we take the special case

$$\psi = \pi/2$$

so that

$$\mathbf{E} = \mathbf{E}_0(\mathbf{i}\cos(\omega t) + \mathbf{j}\sin(\omega t)) \quad (12)$$

This type of electric field produces the torque

$$-\mu \times \mathbf{E} = \mu_z \mathbf{E}_0 \sin(\omega t)\mathbf{i} - \mu_z \mathbf{E}_0 \cos(\omega t)\mathbf{j} - (\mu_x \mathbf{E}_0 \sin(\omega t) - \mu_y \mathbf{E}_0 \cos(\omega t))\mathbf{k} \quad (13)$$

on each of the 108 molecules used in the computer simulation. The latter is used to investigate the effect of this type of torque on dynamical quantities of interest, especially the ccf $C_1(t)$.

Analytical Theory

The purpose of this section is to show analytically that the appearance of $C_1(t)$ in the laboratory frame means that measurable power absorption spectra in the far-infrared region must have a different frequency dependence parallel and perpendicular to the imposed homogeneous electric field (E). The effect of the torque

$$-\mu \times \mathbf{E}$$

can be incorporated in a generalized Langevin equation for the diffusion process as[1,4-6]

$$\frac{d}{dt}C(t) = \lambda(t)C(t) - \int_0^t \phi(t-\tau)C(\tau) \quad (14)$$

Equation 14 is derived from the Liouville equation of classical dynamics by the use of projection operators, as first demonstrated by Mori. In the analysis that follows the memory kernel is treated in the zeroth approximation by using a matrix of friction coefficients. In other words, the matrix equation (14) is used in the Markovian approximation with an additional Mori resonance term representing the effect of the external electric field. The usual linear Mori procedure expands the memory kernel in terms of further memory functions, which in the present context would be matrices of unknown coefficients. Laplace transformation generates the well-known Mori continued fraction, in this case of matrices. This leads to a closer approximation of the rotation/translation diffusion dynamics at the expense of introducing many parameters. The zero-order (matrix Markovian) approximation used in this paper is the simplest possible commensurate with the task at hand, i.e., of describing statistically interdependent rotational and translational molecular diffusion with tractable analytical theory. Further detailed discussion of the properties of eq 14 can be found in ref 4–6. In the present context the matrix Markovian approximation is justified a posteriori by its (albeit limited) success in describing the results of our computer simulation in terms of as few adjustable parameters as possible.

Equation 14 governs the time evolution of the correlation matrix

$$C(t) = \begin{bmatrix} \langle \mathbf{v}(t)\mathbf{v}^T(0)\rangle & \langle \mathbf{v}(t)\boldsymbol{\omega}^T(0)\rangle \\ \langle \boldsymbol{\omega}(t)\mathbf{v}^T(0)\rangle & \langle \boldsymbol{\omega}(t)\boldsymbol{\omega}^T(0)\rangle \end{bmatrix} \quad (15)$$

The interaction

$$-\mu \times \mathbf{E}$$

appears in eq 14 through the matrix $\lambda(t)$:

$$\lambda = i\omega_1 \begin{bmatrix} \mathbf{0} & \mathbf{0} \\ \mathbf{0} & \mathbf{1} \end{bmatrix} \quad (16)$$

where $\mathbf{0}$ is the 3 × 3 null matrix and $\mathbf{1}$ the unit matrix, with the scalar frequency[18]

$$\omega_1 = (\mu E_z/I)^{1/2} \quad (17)$$

The structure of eq 14–17 means that we are dealing with a situation as follows: (1) The three molecular moments of inertia are put equal, so that the dynamics of the molecule are those of the "spherical top" with moment of inertia I. (i) It is assumed

(14) Evans, G. J. *Mater. Lett.* **1984**, *2*, 420.
(15) Evans, M. W. *J. Chem. Phys.* **1982**, *76*, 5473, 5480; *J. Chem. Phys.* **1983**, *77*, 4632; *J. Chem. Phys.* **1983**, *78*, 925, 5403.
(16) Baranova, N. B.; Zeldovich, B. Y. *Chem. Phys. Lett.* **1978**, *57*, 435. Baranova, N. B.; Bogdanov, Y. V.; Zeldovich, B. Y. *Opt. Commun.* **1978**, *22*, 243.
(17) Evans, M. W. *J. Chem. Soc., Chem. Commun.* **1983**, 169.
(18) Evans, M. W.; Grigolini, P.; Marchesoni, F. *Chem. Phys. Lett.* **1983**, *95*, 544, 548.

that the molecular carries a net dipole moment μ which interacts with the external field **E** according to eq 17. (3) There is no direct influence on the linear center of mass velocity (**v**) of the homogeneous electric field **E**, so that terms in λ involving **v** vanish.

It is described fully elsewhere that this set of equations leads to the following results for the Laplace transform of the velocity acf:[1]

$$C^{zz}_{\omega\omega}(p) = \frac{\langle \omega_z{}^2 \rangle}{p - i\omega_1 + \phi^{zz}_{\omega\omega}} \tag{18}$$

$$C^{xx}_{\omega\omega}(p) = \frac{\langle \omega_x{}^2 \rangle (p + \phi^{xx}_{\nu\nu})}{(p + \phi^{xx}_{\nu\nu})(p - 1\omega_1 + \phi^{xx}_{\omega\omega}) + \phi^{xy}_{\nu\omega}{}^2} \tag{19}$$

In these equations $\langle \omega_x{}^2 \rangle$ and $\langle \omega_z{}^2 \rangle$ are mean square angular velocities perpendicular and parallel to the electric field, $\phi^{zz}_{\omega\omega}$ and $\phi^{xx}_{\omega\omega}$ are rotational friction coefficients parallel and perpendicular to the field, $\phi^{zz}_{\nu\nu}$ and $\phi^{xx}_{\nu\nu}$ are the equivalent translational friction coefficients, and $\phi^{xy}_{\nu\omega}$ is the cross coefficient between rotation and translation.

It is clear from eq 18 and 19 that the functions $C^{zz}_{\omega\omega}(p)$ and $C^{xx}_{\omega\omega}(p)$ of the Laplace variable[4] p are different parallel and perpendicular to the field. The isotropy of the system is recovered only when ω_1 and $\phi^{xy}_{\nu\omega}$ both vanish simultaneously. Making the substitution $p = -i\omega$, where ω is the angular frequency in rad s^{-1}, the real and imaginary parts of the angular velocity spectrum $C^{xx}_{\omega\omega}(-i\omega)$ can be recovered. These are illustrated in Figure 1 as a function of ω_1 and $\phi^{xy}_{\nu\omega}$. Figure 1 is essentially the spectrum of the angular velocity acf in the direction perpendicular to the field **E**. It is interesting to note that the real part of this spectrum, multiplied by the factor ω^2, is approximately the equivalent far-infrared power absorption (cf. Figure 3d). When ω_1 and $\phi^{xy}_{\nu\omega}$ both vanish, the real part of $C^{xx}_{\omega\omega}(-i\omega)$ is a Lorentzian. For finite **E** the frequency ω_1 and the friction $\phi^{xy}_{\nu\omega}$both exist in the laboratory frame, and it is reasonable to assume that they are proportional, as discussed elsewhere.[1] These parameters help to define the nature of the nonvanishing elements of $\boldsymbol{C}_1(t)$ from the analytical theory and affect the real part of the angular velocity spectrum as shown in Figure 1. This spectrum has an interesting behavior as a function of $\phi^{xy}_{\nu\omega}/\omega_1$ as this ratio is increased. It is clear from Figure 1a that a secondary high-frequency process appears as the ratio increases up to a point where this dominates the spectrum in the form of a sharp and intense high-frequency peak. The same process is visible in the imaginary part of the spectrum, the dispersion, Figure 1b.

The frequency dependence of the dielectric loss is given approximately by the curves of Figure 1a multiplied by the angular frequency, ω, and that of the dielectric permittivity by those of curve of Figure 1b multiplied by ω and added to the static permittivity. Therefore it is clear from Figure 1 that the appearance of $\boldsymbol{C}_1(t)$ in the laboratory frame of reference is accompanied analytically in the simplest case by the appearance of a peak on the high-frequency side of the dielectric loss. This peak (or, more generally, peaks) is observable in the far-infrared range of frequencies and is produced by computer simulation later in this paper (Figure 3d).

Computer Simulation Algorithms

The equations of motion for 108 CH_2Cl_2 molecules are solved simultaneously for the rotational and translational motions with the constant-volume computer simulation with the usual periodic boundary conditions. The intermolecular pair potential is a 3 × 3 site–site potential composed of Lennard-Jones and partial charge terms, defined by

$$\sigma(\text{Cl–Cl}) = 3.35 \text{ Å}; \quad \epsilon/k(\text{Cl–Cl}) = 173.5 \text{ K}$$

$$\sigma(\text{CH}_2\text{–CH}_2) = 3.96 \text{ Å}; \quad \epsilon/k(\text{CH}_2\text{–CH}_2) = 70.5 \text{ K}$$

$$q_{\text{Cl}} = -0.151 \text{ e}; \quad q_{\text{CH}_2} = 0.302 \text{ e}$$

The simulations were carried out at 296 K with a molar volume of 8×10^{-5} m^3 mol^{-1}. The various types of external force field described already in this paper were written into the algorithm

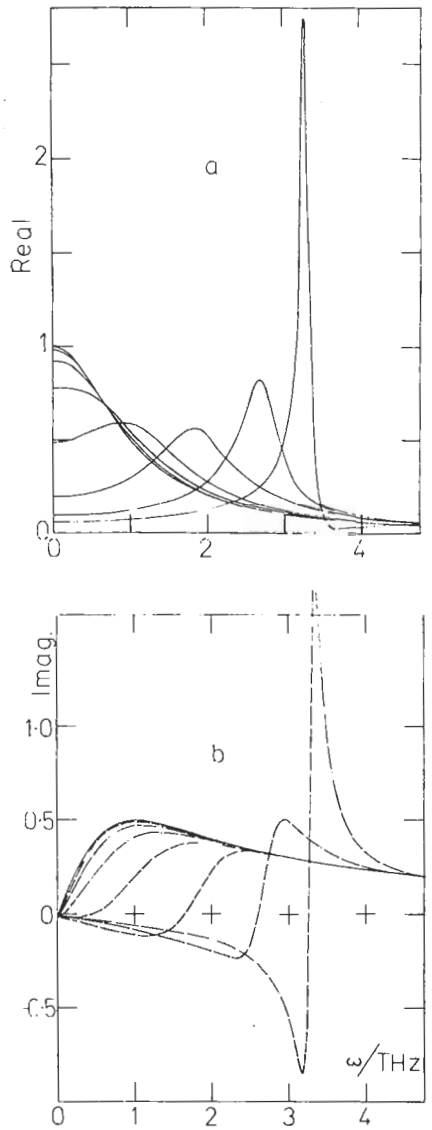

Figure 1. Real part of the angular velocity spectrum $C^{xx}_{\omega\omega}(-i\omega)$ from 19. With $\phi^{xx}_{\nu\nu} = \phi^{xx}_{\omega\omega} = 1.0$ THz; from top to bottom on the left-hand side: $\phi^{xy}_{\nu\omega} = 0$, $\omega_1 = 0$ (Lorentzian); $\phi^{xy}_{\nu\omega} = 0.1$ THz, $\omega_1 = 0.01$ THz; $\phi^{xy}_{\nu\omega} = 0.25$ THz, $\omega_1 = 0.025$ THz; $\phi^{xy}_{\nu\omega} = 0.50$ THz, $\omega_1 = 0.05$ THz; $\phi^{xy}_{\nu\omega} = 1.0$ THz, $\omega_1 = 0.10$ THz; $\phi^{xy}_{\nu\omega} = 2.00$ THz, $\omega_1 = 0.20$ THz; $\phi^{xy}_{\nu\omega} = 3.0$ THz, $\omega_1 = 0.30$ THz; $\phi^{xy}_{\nu\omega} = 3.70$ THz, $\omega_1 = 0.37$ THz. (a) Real part: ordinate, $(C^{xx}_{\omega\omega}(-i\omega))$; abscissa, ω/THz. (b) imaginary part: ordinate, $(C^{xx}_{\omega\omega}(-i\omega))$; abscissa, ω/THz.

at the point where the intermolecular forces and torques are defined. This method is described fully in the literature and allows the computation of rise transients (averages, for example, over the orientation vectors $\mathbf{e}_1$, $\mathbf{e}_2$, and $\mathbf{e}_3$ of the principal molecular moment of inertia frame). If the liquid is birefringent, then these transients are different in the x and z axes of the laboratory frame. Similar averages of the laboratory-frame components of the linear center of mass velocity provide a method of seeing whether the sample as a whole is translating, and in what direction.

After applying the external field and allowing the transients to reach their field-on equilibrium level, it is then possible to compute and investigate the nonvanishing elements of ccf's such as

$$\boldsymbol{C}_2(t) = \langle \dot{\mu}(t)\mathbf{v}^{\mathrm{T}}(0) \rangle$$

and $\boldsymbol{C}_1(t)$ in the laboratory frame (x, y, z).

The magnitude of the external electric field gradient was in energetic terms more than equivalent to the thermal energy per molecule, kT, and was sufficient to saturate the Langevin function. The energy pumped into the system by the external field gradient was +21.4 kJ/mol, raising the natural internal energy of the 108 dichloromethane molecules from −37.2 to −15.8 kJ/mol. This is

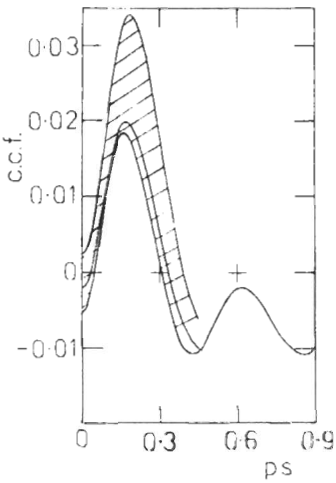

Figure 2. Laboratory-frame ccf element $\langle v_x(t)\dot{e}_{1z}(0)\rangle/(\langle v_x^2\rangle^{1/2}\langle \dot{e}_{1z}^2\rangle^{1/2})$ from computer simulation. Ordinate, $\langle v_x(t)\dot{e}_{1z}(0)\rangle/(\langle v_x^2\rangle^{1/2}\langle \dot{e}_{1z}^2\rangle^{1/2})$.

a much bigger field gradient than that usually available in the laboratory. However, the theoretical work of Born[8] and its experimental confirmation by Lertes[10] has shown that weak electric fields are sufficient to produce a rotational macroscopic torque in a molecular liquid under the right conditions. The difference between the work of Lertes and the present computer simulation is of course sample size. The sample of molecular liquid suspended by Lertes on this torsion wire contained many orders of magnitude more molecules than the 108 used in this simulation. In both Lertes' experiment and in our computer simulation the electric field acted on the molecules of the liquid sample. In the simulation, however, the small sample size rules out proper consideration of cooperativity and makes it necessary to use strong external fields to see what is being sought above the background thermal noise.

Similarly, the torque due to the rotating electric field was, for the purposes of the present computer simulation, energetically equivalent to about $10.0kT$ and applied at the molecular level. The effect of a torque of type (11) is to put each molecule locally into a rotating motion following the field. This motion has been animated on videotape in this laboratory and can be seen clearly superimposed on the molecular motion fueled by the thermal kinetic energy. With this type of motion the effect of the periodic boundary conditions is no more of a problem than in thermal motion. The rotating electric field acts on each molecule in unison and in a large enough sample (as used by Lertes) generates a torque on a macroscopic scale. In order to simulate the rotation actually seen macroscopically by Lertes, periodic boundary conditions in four sides of the box would have to removed and replaced by hard walls.

After application of the external electric field or field gradient, the sample is brought to field-on equilibrium with the use of periodic temperature rescaling. The effect of the temperature rescaling was to introduce discontinuities into the translational and rotational kinetic energies. During the rise transient (equilibration) interval following upon the application of the external field, these discontinuities sometimes worked themselves though into orientational averages such as those in eq 5, but varying the temperature rescaling interval showed that temperature rescaling was not responsible for the oscillations observed in this and other work of this nature and illustrated in Figure 5, for example.

Cross Correlation between Rotation and Translation

It is possible that a whole range of new laboratory-frame ccf's are generated in a birefringent liquid in the presence of a z axis homogeneous electric field. The first two to be discovered were[1]

$$C_{tr}^{xy} = \langle v_x(t)\omega_y(0)\rangle/(\langle v_x^2\rangle^{1/2}\langle \omega_y^2\rangle^{1/2})$$

and

$$C_{tr}^{yx} = \langle v_y(t)\omega_x(0)\rangle/(\langle v_y^2\rangle^{1/2}\langle \omega_x^2\rangle^{1/2})$$

which are mirror images in time dependence and which determine

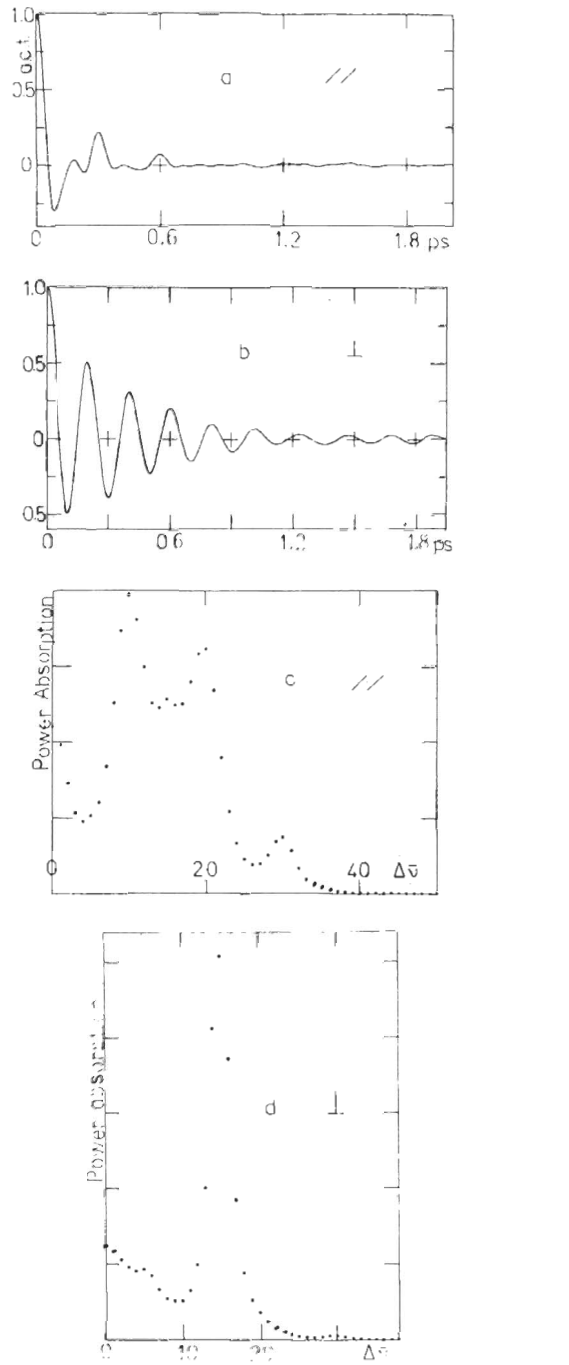

Figure 3. (a) Laboratory-frame rotational velocity acf $\langle \dot{e}_{3z}(t)\dot{e}_{3z}(0)\rangle/\langle \dot{e}_{3z}^2\rangle$ parallel to the electric field (**E**). (b) Laboratory-frame rotational velocity ccf $\langle \dot{e}_{3x}(t)\dot{e}_{3x}(0)\rangle/\langle (\dot{e}_{3x}^2\rangle$ perpendicular to the electric field (**E**). (c) Far-infrared power absorption spectrum from (a). (d) Far-infrared power absorption spectrum from (b). Ordinates: (a) $\langle \dot{e}_{3z}(t)\dot{e}_{3z}(0)\rangle/\langle \dot{e}_{3z}^2\rangle$; (b) $\langle \dot{e}_{3x}(t)\dot{e}_{3x}(0)\rangle/\langle \dot{e}_{3x}^2\rangle$ ((a and b) There is a cut-off effect at $\Delta\bar{\nu} = 0$); (c) power absorption (arbitrary scale); (d) power absorption (arbitrary scale). Abscissas: (a) time/ps; (b) time/ps; (c) $\Delta\bar{\nu} = 100/72$ cm^{-1}; (d) $\Delta\bar{\nu} = 100/72$ cm^{-1}.

the symmetry of the off-diagonal elements of the matrix $\boldsymbol{C}(t)$ in eq 15. In this section we report for the first time the existence in the laboratory frame of an element of $\boldsymbol{C}_2(t)$, the ccf between the time derivative of the dipole moment vector and center of mass linear velocity $\mathbf{v}$. Note that none of the ccf's are considered in standard linear response theory[5,6] (in the Onsager reciprocal relations or in Onsager thermodynamics in general). Their existence in the presence of electric or electromagnetic fields is therefore a step forward in our understanding of the molecular dynamics of the condensed states of matter.

During the course of this work it was found that ccf's existed between all three orientation vectors and $\mathbf{v}$. The symmetries of

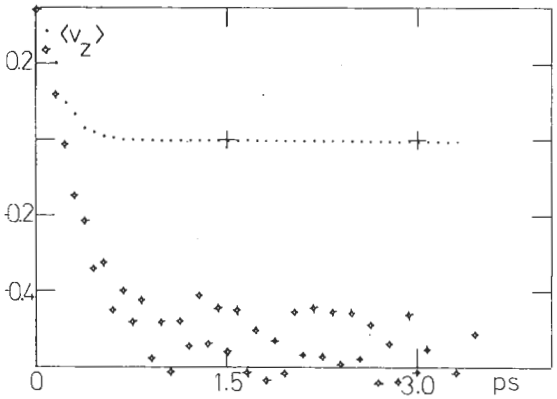

Figure 4. Velocity drift $\langle v_z \rangle$ (⊙) and $\langle v_x \rangle$ (●) created by the force defined in eq 6. Ordinate: mean velocity (reduced units) abscissa: time/ps.

these ccf's are different from that of $C_1(t)$. In Figure 2 we illustrate the ccf element

$$\langle v_x(t)\dot{e}_{1z}(0)\rangle / (\langle v_x^2\rangle^{1/2}\langle \dot{e}_{1z}^2\rangle^{1/2})$$

from three independent runs. The hatching in this figure therefore illustrates the noise level. In contrast to C_{tr}^{xy} and C_{tr}^{yx}, this element does not have a mirror image and seems to be the only element visible above the background noise in the 3 × 3 ccf matrix:

$$\langle v(t)\dot{e}_1{}^{T}(0)\rangle$$

The appearance of ccf's such as these in the presence of birefringence (caused by an external homogeneous electric field **E**) can be investigated experimentally by measuring the far-infrared power absorption parallel and perpendicular to the field. The spectra are essentially the Fourier transforms of, in our notation, the rotational velocity acf's

$$\langle \dot{e}_{3z}(t)\dot{e}_{3z}(0)\rangle$$

and

$$\langle \dot{e}_{3x}(t)\dot{e}_{3x}(0)\rangle$$

respectively. Naturally the same equations of motion produce both acf's and ccf's, and therefore experimental data from the far infrared provide us with information on the ccf's themselves. The acf's

$$\langle \dot{e}_{3z}(t)\dot{e}_{3z}(0)\rangle$$

and

$$\langle \dot{e}_{3x}(t)\dot{e}_{3x}(0)\rangle$$

and their Fourier transforms (the far-infrared spectra) are illustrated in Figure 3 in the presence of a strong z axis homogeneous electric field **E**. The spectra are clearly different in frequency dependence and are also richly structured with peaks (Figure 3d). The liquid is therefore birefringent.

The Simulation of Birefringence in a Field Gradient

By using eq 6 it is possible with the simulation technique to isolate the effect of a field gradient del **E** from that of the field **E**. The force defined in eq 6 leads to the mean center of mass velocity (z component) in Figure 4. At the same time the x component falls nearly to zero. It is clear, therefore, that the sample of 108 molecules is drifting in the z direction in response to the imposed force defined in eq 6. This flow produces the birefringence measured in Figure 5 through the first- and second-order orientational averages from eq 11. This is a verification by computer simulation of the well-known phenomenon of flow-induced birefringence,[9] the linear flow in this case being due to an imposed electric field gradient.

Vortex Flow and Laboratory-Frame Ccf's

The pioneering experimental results of Lertes[10] and later Grossetti[11] interpreted by Born[8] and later by Dahler[9] indicate that

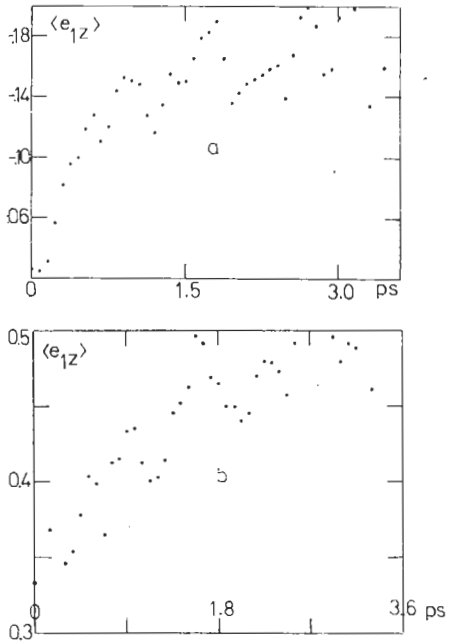

Figure 5. Development of orientational averages (a) $\langle e_{1z} \rangle$ and (b) $\langle e_{1z}^2 \rangle$ in response to the force defined in eq 6. Ordinates: (a) $\langle e_{1z} \rangle$; (b) $\langle e_{1z}^2 \rangle$. Abscissa: ps.

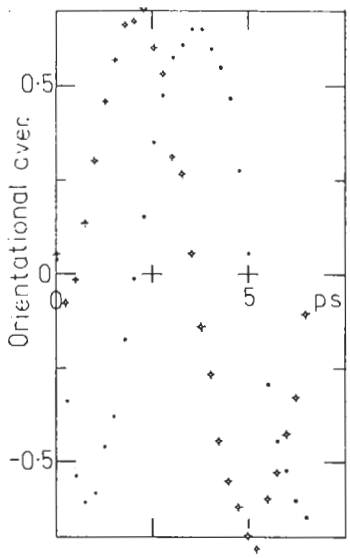

Figure 6. Orientational averages $\langle e_{1x} \rangle$ (⊙) and $\langle e_{1y} \rangle$ (●) in response to a rotating electric field (ω = 1.0 THz). Ordinate: first-order orientational averages. Abscissa: time/ps.

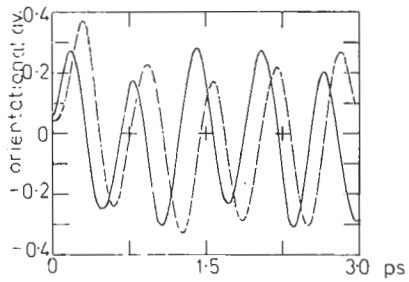

Figure 7. As for Figure 6: —, $\langle e_{1x} \rangle$; ---, $\langle e_{1y} \rangle$; ω = 10.0 THz. Ordinate: first-order orientational average. Abscissa: time/ps.

a rotating electric field of the type (11) or (12) should produce a vortex flow (i.e., a whirlpool effect) which is generated on a fundamental level by a torque of the type (16) on each molecule.

Figure 6 is an illustration of the vortex flow for an angular frequency of 1.0 × 10^{12} rad/s in eq 12, and Figure 7 is the

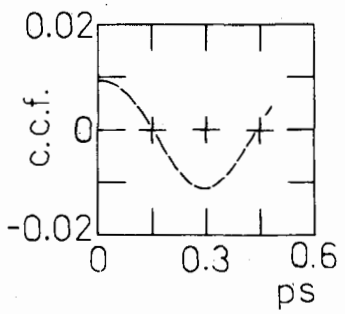

Figure 8. Laboratory-frame ccf element $\langle \nu_x(t)\omega_y(0)\rangle/(\langle \nu_x^2\rangle^{1/2}\langle \omega_y^2\rangle^{1/2})$ in the presence of a rotating electric field. Ordinate: $\langle \nu_x(t)\omega_y(0)\rangle/(\langle \nu_x^2\rangle^{1/2}\langle \omega_y^2\rangle^{1/2})$. Abscissa: time/ps.

equivalent for 10.0×10^{12}. Both figures are given in terms of the three orientational averages

$$\langle e_{1x}\rangle \quad \langle e_{1y}\rangle \quad \langle e_{1z}\rangle$$

The first two are oscillatory and out of phase (Figures 6 and 7), while the third remains close to zero within the noise. The z axis is therefore the symmetry axis of the whirlpool, and the x and y directions define the helical nature of the orientational order imposed by the external electric field (12) and set up by the four metal plates external to the sample. The hydrodynamics of this situation are described in great detail by Born[8] and by Dahler,[9] who anticipated a dispersion effect as the angular frequency passes through a maximum defined by $\omega\tau = 1$, where τ is the Debye relaxation time. Lertes[10] and Grosetti[11] did not have available to them a field frequency high enough to see this effect, but it can be seen clearly in Figures 6 and 7. As the angular frequency is increased from 1.0 to 10.0 rad/sec. the amplitude of the time dependent oscillatory averages $\langle e_{1x}\rangle$ and $\langle e_{1y}\rangle$ is seen to decrease, a clear indication of dispersion.

Finally, in Figure 8 we illustrate the ccf element $\langle \nu_x(t)\omega_y(0)\rangle/(\langle \nu_x^2\rangle^{1/2}\langle \omega_y^2\rangle^{1/2})$ under a rotating field of frequency 1.0 THz. Therefore, it seems clear that a vortex flow is also capable of generating laboratory frame ccf's which do not appear in classical linear response theory.

Acknowledgment. The University of Wales is thanked for the University and Pilcher Senior Fellowships.

Mass Transfer Phenomena Studied by Reversed-Flow Gas Chromatography. 2. Mass Transfer and Partition Coefficients across Gas–Solid Boundaries

N. A. Katsanos,* P. Agathonos, and A. Niotis

Physical Chemistry Laboratory, University of Patras, Patras, Greece *(Received: July 10, 1987; In Final Form: September 30, 1987)*

Rate constants, partition ratios, partition coefficients, and overall mass transfer coefficients for the distribution of two solute hydrocarbons (propene and butane) between gas and solid phases have been determined at various temperatures. The mathematical model and its solution were based on the reversed-flow gas chromatography technique, leading again to the same form of equation as before. This equation, describing the height of the chromatographic sample peaks as a function of time, was used to analyze the experimental data and calculate the values of the various coefficients above. There is not a big difference between the results of the present and the previous work for comparable systems.

Introduction

In the first paper of this series[1] the reversed-flow gas chromatography technique was applied to the determination of mass transfer and partition coefficients of gases across gas–liquid boundaries. These coefficients are useful in chromatographic separations and other operations of chemistry and chemical engineering. Their determination was based on repeatedly reversing the direction of the carrier gas flowing through an empty chromatographic tube (4-mm i.d.) called a sampling column (cf. Figure 1). The flow reversals are made by means of a four-port valve connected as shown in Figure 1 of ref 1; they are of short duration (10–60 s) and create extra symmetrical peaks (sample peaks) superimposed on the otherwise continuous chromatographic trace. (For an example see Figure 2 in ref 1.)

The height h of these symmetrical sample peaks, measured from the continuous chromatographic signal, is proportional to the concentration of the gaseous solute under study at the junction $x = l'$ (cf. Figure 1) at the time of each flow reversal. This concentration is due to a small gas volume (0.5–1 cm^3) of the solute, introduced through the injector and being allowed to diffuse along the empty cylindrical tube (4-mm i.d.) called a diffusion column. A plot of ln h versus time is termed a diffusion band. It is the distortion of such a band, brought about by the presence of a gas–liquid boundary at the closed end of the diffusion column, that permits the determination of mass transfer and partition coefficients.[1]

In the present work the theme of mass transfer phenomena across phase boundaries is continued by measuring the relevant coefficients across gas–solid boundaries, the solid surface being either bare or covered with a thin liquid film, thus forming a conventional stationary phase of gas–liquid chromatography.

Theoretical Section

The method presented here is again based on the distortion of a diffusion band, but this time the distortion is due to the presence of a solid at one end of the diffusion column, creating a gas–solid boundary, as shown in Figure 1. The mathematical formulation of the problem is somehow different from that of a gas–liquid boundary,[1] because there is no agitation of the solid and there exists a longitudinal diffusion of the solute in the interparticle space of the bed containing the solid. The analysis can be followed by referring to Figure 1, which is similar to Figure 4 of ref 1.

Region z, Diffusion Column. In this region (empty of any solid material) the diffusion equation holds true

$$\partial c_z/\partial t_0 = D\,\partial^2 c_z/\partial z^2 \qquad (1)$$

where $c_z(z,t_0)$ is the concentration of the solute vapor A in region z of the cell at time t_0 and D is the diffusion coefficient of A into

(1) Katsanos, N. A.; Dalas, E. *J. Phys. Chem.* **1987**, *91*, 3103.

0022-3654/88/2092-1645$01.50/0